Nonlinearity 5 (1992) 523–539. Printed in the UK

Action billiards

M A M de Aguiar and A M Ozorio de Almeida
Instituto de Física 'Gleb Wataghin', Universidade Estadual de Campinas, 13081 Campinas, SP, Brazil

Received 12 April 1991, in final form 17 June 1991
Accepted by M V Berry

Abstract. Truncation of the Hamiltonian matrix in the harmonic oscillator representation of quantum mechanics corresponds to cutting off the action dependence of the classical Hamiltonian. The conjugate angle variable suffers a discontinuous jump, when the orbit collides with the action boundary in a manner analogous to the specular reflexion on the border of a common billiard. We derive the connection rule for the angles by analysing the limit of smooth cut-offs in the classical Hamiltonian, for which examples are given. It is found that different definitions of the classical cut-off may lead to diverse orbit structures, though the corresponding finite Hamiltonian matrices are identical.

PACS numbers: 0320, 0365

1. Introduction

In common billiards the classical motion is contained in a finite region of position space (with coordinates q) because there is a boundary at which the normal gradient of the Hamiltonian diverges:

$$\partial H(p, q)/\partial q \to \infty. \tag{1.1}$$

When an orbit hits the boundary, the corresponding momentum therefore jumps to a new value with which it resumes its motion within the allowed region. Usually one considers there the simple Hamiltonian

$$H(p, q) = p^2/2 \tag{1.2}$$

so that the momentum is conserved between the collisions which truly determine the motion. However, modifications of this interior Hamiltonian do not affect in any way the bounce in the momentum. For instance, by introducing a large magnetic field, the motion of charged particles in a billiard will be such that most describe circles with no collisions. The few orbits that hit the boundary are still specularly reflected.

Billiards have proved to be an important model for the study of chaotic classical systems and for the difficult problem of understanding the semiclassical limit of

0951-7715/92/020523 + 17$04.50

corresponding quantum systems. Unfortunately, they are of no help in surmounting the fundamental difficulty that the quantum representation of the Hamiltonian, corresponding to an infinite classical phase space, requires an infinite matrix in any basis. Computation of the eigenenergies and eigenstates therefore relies on an uncontrollable cut-off of this matrix.

The great interest that has ensued in the dynamics of compact phase spaces is therefore understandable. Of these the most studied are torus maps [1, 2], though there is also important work concerning Hamiltonians on a sphere [3]. In these cases the basis is always finite, so that the semiclassical limit can be more reliably envisaged as an extrapolation from increasing though finite matrices.

Our purpose here is to define a new class of dynamical systems for which the quantum matrices are finite. This can be achieved as follows. Consider any given Hamiltonian matrix and the finite block that one effectively diagonalizes. This diagonalization is exact not for our original problem but for a perturbed quantum Hamiltonian such that our chosen block is uncoupled from the rest of the Hamiltonian matrix. Semiclassically, the basis states correspond to basis tori embedded in a set that foliates phase space. A cut-off in the matrix corresponds classically to a cut-off in the dependence of the Hamiltonian on the actions of the tori lying outside a definite region. A sharp cut-off will lead to bounces of the conjugate angle variables.

The resulting classical system is an *action billiard*. Contrary to common billiards, we will be mostly interested in the cases where a large proportion of the classical orbits does not hit the boundary. At first sight, this may seem incompatible with ergodic and therefore chaotic classical motion; however, it must be remembered that the motion can only be ergodic within the energy shell. Hence, if the energy shells are compact, there can be a whole interval of energies for which the classical motion is unaffected by the boundary. What of the orbits that do collide with the boundary? We shall show that the angle bounce can easily be controlled by considering the limit of smooth cut-offs for the Hamiltonian in a simple analogy to normal billiards.

Once the classical cut-off has been established, we may study the semiclassical limit of the corresponding quantized system. The discrete lattice of quantized tori that fit into the action billiard will become tighter, hence the dimension N of the Hamiltonian matrix will grow inversely with Planck's constant, $N \propto \hbar^{-L}$, where L is the number of freedoms, without altering the classical motion. Hence, it is only in the limit $\hbar \to 0$ that $N \to \infty$.

It may appear that the foregoing argument depends intrinsically on some semiclassical definition of the matrix elements [4, 5]. However, we shall show in section 2 that a proper correspondance can be achieved in the case of the occupation number basis of harmonic oscillators. In section 3 we define and exemplify action billiards with a single freedom, whereas the general case will be the subject of section 4.

Our main results concern the classical action billiard. Thus, readers who are not interested in the quantum mechanical motivation can skip most of section 2, from which they need only (2.5), (2.9), (2.16) and (2.17).

2. Classical correspondance of the occupation number basis

Consider an analytical classical Hamiltonian specified by its Taylor series:

$$H(\boldsymbol{p}, \boldsymbol{q}) = \sum_{\substack{l_1,\ldots,l_L \\ m_1,\ldots,m_L}} H_{l,m} p_1^{l_1} \ldots p_L^{l_L} q_1^{m_1} \ldots q_L^{m_L} \tag{2.1}$$

where L is the number of freedoms. The complex canonical transformation

$$\begin{aligned} a_j &= 2^{-1/2}(q_j + \mathrm{i}p_j) \\ a_j^* &= 2^{-1/2}(q_j - \mathrm{i}p_j) \end{aligned} \tag{2.2}$$

takes the Hamiltonian to the form [6]

$$H'(\boldsymbol{a}, \boldsymbol{a}^*) = \sum_{l,m} H'_{l,m} a_1^{l_1} \ldots a_L^{l_L} a_1^{*m_1} \ldots a_L^{*m_L} \tag{2.3}$$

whereas the canonical transformation to polar coordinates

$$\begin{aligned} a_j &= I_j^{1/2} \exp(\mathrm{i}\varphi_j) \\ a_j^* &= I_j^{1/2} \exp(-\mathrm{i}\varphi_j) \end{aligned} \tag{2.4}$$

defines the Hamiltonian

$$H''(\boldsymbol{I}, \boldsymbol{\varphi}) = \sum_{k,r} H''_{k,r} I_1^{r_1/2} \ldots I_L^{r_L/2} \exp(\mathrm{i}\boldsymbol{k} \cdot \boldsymbol{\varphi}). \tag{2.5}$$

Thus, the Hamiltonian (2.5) appears in the appropriate action angle variables for classical cut-offs, whereas we can immediately quantize (2.3) by defining the quantum analogue of (2.2) as the operator equation,

$$\begin{aligned} \hat{a}_j &= 2^{-1/2}(\hat{q}_j + \mathrm{i}\hat{p}_j) \\ \hat{a}_j^+ &= 2^{-1/2}(\hat{q}_j - \mathrm{i}\hat{p}_j) \end{aligned} \tag{2.6}$$

and then substitute these for the equivalent classical variables in (2.3) after some adequate symmetrization [7]. The matrix elements of $\hat{H}$ in the harmonic oscillator representation $|\boldsymbol{n}\rangle$ are simply obtained by use of the well-known formulae [8]

$$\begin{aligned} \hat{a}_j |\boldsymbol{n}\rangle &= (\hbar n_j)^{1/2} |n_1, \ldots, n_j - 1, \ldots, n_L\rangle \\ \hat{a}_j^+ |\boldsymbol{n}\rangle &= (\hbar(n_j + 1))^{1/2} |n_1, \ldots, n_j + 1, \ldots, n_L\rangle. \end{aligned} \tag{2.7}$$

In the special case where (2.1) is a polynomial, we obtain an infinite matrix $\langle \boldsymbol{n}' | \hat{H} | \boldsymbol{n} \rangle$ that has zero elements far from the diagonal. The relation between the indices in (2.3) and (2.5) is simply

$$\begin{aligned} r_j &= l_j + m_j \\ k_j &= l_j - m_j \end{aligned} \tag{2.8}$$

so that all the terms in (2.5) with a specific $\boldsymbol{k}$ determine the elements in a given line parallel to the main diagonal in the Hamiltonian matrix.

We can now generate the perturbation that uncouples a given block by working directly with the Hamiltonian. Consider an analytical hat function $\Phi_\lambda(\boldsymbol{I})$, such that $\Phi_\lambda < \varepsilon$ outside a given region and $1 \geqslant \Phi_\lambda > 1 - \varepsilon$ inside and the width of the boundary in which $\varepsilon \leqslant \Phi_\lambda \leqslant 1 - \varepsilon$ shrinks as $\lambda \to 0$ for arbitrarily small ε. We can identify its Taylor series

$$\Phi_\lambda(\boldsymbol{I}) = \sum_s \Phi_{\lambda,s} I_1^{s_1} \ldots I_L^{s_L} \tag{2.9}$$

as a special case of the classical representation (2.5) and hence obtain

$$\Phi_\lambda(\boldsymbol{a}, \boldsymbol{a}^*) = \sum_s \Phi_{\lambda,s} (a_1 a_1^*)^{s_1} \ldots (a_L a_L^*)^{s_L} \tag{2.10}$$

via the transformation (2.4). Thus, we define the corresponding operator

$$\hat{\Phi}_j = \sum_s \Phi_{\lambda,s}(\hat{a}_1\hat{a}_1^+)^{s_1} \ldots (\hat{a}_L\hat{a}_L^+)^{s_L} \tag{2.11}$$

which is diagonal in the occupation number basis:

$$\langle n'| \hat{\Phi}_\lambda |n\rangle = \delta_{nn'} \Phi_\lambda[(n + \tfrac{1}{2})h]. \tag{2.12}$$

In the limit where $\lambda \to 0$ then we can simply identify

$$\hat{\Phi}_0 = \sum_{n=0}^{N} |n\rangle\langle n| \tag{2.13}$$

that is, $\hat{\Phi}_0$ is simply the projection operator onto the finite number of states whose corresponding actions lie inside the classical billiard.

It is now evident that our quantum Hamiltonian operator for a single block of the original matrix is just

$$\hat{H}_0 = \hat{\Phi}_0 \hat{H} \hat{\Phi}_0 \tag{2.14}$$

which can be considered as the limit of the 'smooth' Hamiltonian

$$\hat{H}_\lambda = \hat{\Phi}_\lambda \hat{H} \hat{\Phi}_\lambda \tag{2.15}$$

which, in its turn, corresponds to the classical Hamiltonian

$$H''_\lambda(\boldsymbol{I}, \varphi) = H''(\boldsymbol{I}, \varphi)(\Phi_\lambda(\boldsymbol{I}))^2. \tag{2.16}$$

The action billiard is therefore the limit of H''_λ as $\lambda \to 0$.

Having identified $\hat{\Phi}$ with the projection operator, we see that it is wholly irrelevant to quantum mechanics how we define our Hamiltonian for other values of n, as long as the Hamiltonians in each region are not coupled. However, we shall find that this possibility can alter the classical motion for those orbits that hit the billiard boundary, so we shall also consider Hamiltonians of the form

$$H(\boldsymbol{I}, \varphi) = H''(\boldsymbol{I}, \varphi)[\Phi_\lambda(\boldsymbol{I})]^2 + H'''(I, \varphi)[\Phi'_\lambda(\boldsymbol{I})]^2 \tag{2.17}$$

where $H'''(\boldsymbol{I}, \varphi)$ is some different Hamiltonian and $\Phi'_\lambda(\boldsymbol{I})$ is the hat function for the complementary volume in phase space and hence corresponds to the projection operator for the infinite complementary set of states $|n\rangle$ as $\lambda \to 0$.

3. One-dimensional action billiards

The motion in common billiards reduces for one dimension to the trivial problem of a particle in a box. Though this is usually analysed only in quantum mechanics, we can obtain the classical reflection rule at the boundary by considering the limit of smooth ever steeper potentials [8].

In the case of an action billiard, we consider the Hamiltonian $H(I, \varphi)$, Whose phase curves can be obtained by solving

$$H(I, \varphi) = E \tag{3.1}$$

for $I_E(\theta)$. The simplest action billiard is then defined as

$$H_0(I, \varphi; \mathcal{I}) = H(I, \varphi)(\Theta_0(\mathcal{I} - I))^2 = \begin{cases} H(I, \varphi) & (I \leqslant \mathcal{I}) \\ 0 & (I > \mathcal{I}) \end{cases} \tag{3.2}$$

where $\Theta_0(x)$ is the unit step function.

The orbits of the original system move along its continuous phase curves, which for some energies will be cut by the boundary $I = \mathcal{I}$, as shown in figure 1. The only problem is to determine the branch of $I_E(\varphi)$ to which the orbit will jump instantaneously. To this end we analyse the smoothed billiard

$$H_\lambda(I, \varphi; \mathcal{I}) = H(I, \varphi)(\Theta_\lambda(\mathcal{I} - I))^2 \tag{3.3}$$

where Θ_λ is a smoothed step of width λ.

The trajectories are the solution of Hamilton's equations:

$$\begin{aligned} \dot{I}_\lambda &= -\frac{\partial H_\lambda}{\partial \varphi} = \frac{-\partial H(I, \varphi)}{\partial \varphi}(\Theta_\lambda(\mathcal{I} - I))^2 \\ \dot{\varphi}_\lambda &= \frac{\partial H_\lambda}{\partial I} = \frac{\partial H(I, \varphi)}{\partial I}(\Theta_\lambda(\mathcal{I} - I))^2 + H(I, \varphi)\frac{\mathrm{d}}{\mathrm{d}I}(\Theta_\lambda(\mathcal{I} - I))^2. \end{aligned} \tag{3.4}$$

The second term of $\dot{\varphi}$ diverges in the limit $\lambda \to 0$, whereas the other terms in the phase velocity remain finite. Hence, the billiard limit generates very fast motion in the direction parallel to the boundary.

A first impression could then be that the boundary merely 'squashes the phase curves', but this need not be so. For instance, it is usual to have $H(I, \varphi)$ positive and growing with I, so that $\dot{\varphi} > 0$. However, $\Theta_\lambda(\mathcal{I} - I)$ decreases with I so that $\dot{\varphi}_\lambda < 0$. Thus, in this case the phase curves actually close in the opposite direction to that of continuous squashing, as shown in figure 2. This feature can be understood as the creation of pairs of stable and unstable equilibria near the boundary: moving up in action along the $\varphi = \pi$ line in figure 1 we are climbing up a valley, whereas we ascend a ridge along the $\varphi = 0$ line. In the first case, the sudden decline generates a col, whereas the ridge attains a maximum before the forced descent.

We conclude that the billiard limit may involve the presence of degenerate equilibria at points where the phase curve is tangential to the boundary. Even so, neighbouring points jump instantaneously to a neighbouring branch of $I_E(\theta)$. The

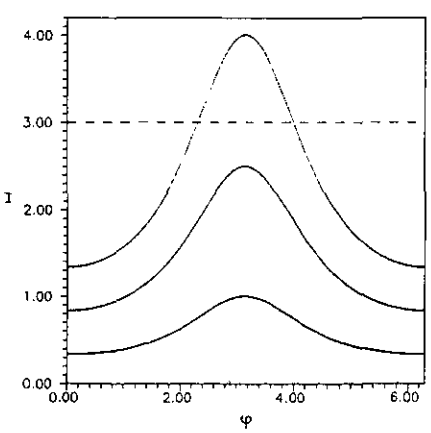

Figure 1. $I \times \varphi$ level curves for the Hamiltonian of (3.6) with $a = 0.5$. The dotted line at $I = 3.0$ is where the Hamiltonian will be truncated.

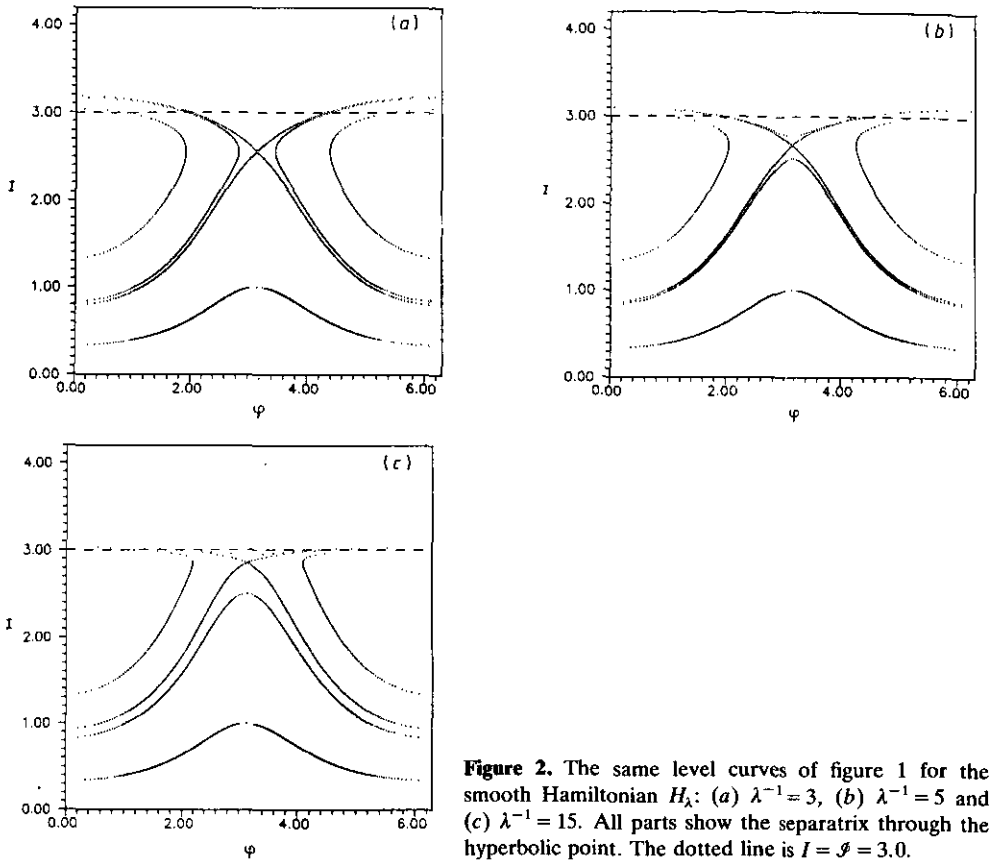

Figure 2. The same level curves of figure 1 for the smooth Hamiltonian H_λ: (*a*) $\lambda^{-1}=3$, (*b*) $\lambda^{-1}=5$ and (*c*) $\lambda^{-1}=15$. All parts show the separatrix through the hyperbolic point. The dotted line is $I=\mathcal{I}=3.0$.

choice of direction for the jump in the case of Hamiltonian (3.2) depends on the sign of H.

The presence of degenerate equilibria on the billiard boundary can be eliminated by the use of more general billiards such as (2.17). An alternative to (3.3) is

$$H_\lambda(i, \varphi; \mathcal{I}) = H(I, \varphi)(\Theta_\lambda(\mathcal{I}-I))^2 + A(\Theta_\lambda(I-\mathcal{I}))^2. \tag{3.5}$$

Thus, if the constant A is chosen larger than $H(\mathcal{I}, \varphi)$ for any φ, the slope of H_λ to the boundary is always positive, so that there are no equilibria for $I<\mathcal{I}$. The topology of the classical orbits can therefore be completely different in the two cases, though the corresponding finite quantum matrices are identical!

We will now illustrate the action billiard with a concrete example. Let

$$H(I, \varphi) = I(1 + a\cos\varphi) \qquad a<1. \tag{3.6}$$

The orbits are level curves of $H(I, \varphi)$,

$$I_E(\varphi) = \frac{E}{1+a\cos\varphi}$$

and three of them are shown as figure 1.

To form our action billiard we choose $\mathcal{I}=3.0$ in (3.2).

The jump $\Delta\varphi$ can be immediately obtained from

$$\mathcal{I}(1 + a\cos\varphi_i) = \mathcal{I}(1 + a\cos\varphi_f)$$

or

$$\varphi_f = 2\pi - \varphi_i.$$

The three corresponding curves of H_0 in figure 1 can then be identified: the two curves that do not touch the wall at $\mathcal{I} = 3.0$ are not affected, and the third curve is made of the two pieces below $\mathcal{I}$ connected by a straight line from $(\mathcal{I}, \varphi_i)$ to $(\mathcal{I}, \varphi_f)$ that is traversed in zero time.

Now consider the smooth version H_λ by replacing the step function by

$$\Theta_\lambda = \frac{1 - \tanh \lambda^{-1}(I - \mathcal{I})}{2}.$$

As λ goes to zero, Θ_λ approaches to $\Theta_0(I - \mathcal{I})$.

In figure 2 we show the same three curves of figure 1 for three different values of λ and verify the appearance of two new equilibria (not present in H). The separatrices through the unstable point are also displayed in the figures. This can be seen directly from the equation of motion:

$$\dot{\varphi} = (1 + a \cos \varphi)\left(\Theta_\lambda^2 - \frac{\lambda^{-1} I \Theta_\lambda}{\cosh^2 \lambda^{-1}(I - \mathcal{I})}\right)$$

$$\dot{I} = -Ia \sin \varphi \Theta_\lambda^2.$$

For non-zero λ we find $\dot{\varphi} = \dot{I} = 0$ for $\varphi = 0, \pi$ and

$$\Theta_\lambda - \frac{\lambda^{-1} I}{\cosh^2 \lambda^{-1}(I - \mathcal{I})} = 0.$$

In the limit of small λ, this can be approximated by the simpler transcendental equation

$$4I\lambda^{-1} = e^{2\lambda^{-1}}(I - \mathcal{I})$$

which means that as $\lambda \to 0$, $I \to \mathcal{I}$ and the separatrix passing through $\varphi = \pi$ coincides with the orbit of H that is tangential to the line $I = \mathcal{I}$. Therefore, this cut-off introduces an island structure that, for finite λ, allows for tunnelling in the quantum mechanical picture! Besides, the level curves above the unstable equilibrium look very much like a harmonic oscillator with a large frequency.

Next we illustrate the alternative cut-off of (3.5). Figure 3 shows the same level curves for the case of $A = 5.0$, and the squashing effect replaces the equilibrium points of the previous figure.

As a last one-dimensional example we show the orbits for the system

$$H_\lambda = I(1 + a \cos 2\varphi)\Theta_\lambda^2(I - \mathcal{I}). \tag{3.7}$$

In this case the orbits of $H_0 = I(1 + a \cos 2\varphi)$ that cross the wall $I = \mathcal{I}$ will do so twice. The effect of this double crossing in H_λ is shown in figure 4 for $\lambda^{-1} = 15$, where two islands are generated.

Notice, however, that the initial trajectory oscillating back and forth twice has split into two separate orbits at the same energy. The equation for θ_f in terms of θ_i is, in this case,

$$\cos 2\varphi_i = \cos 2\varphi_f$$

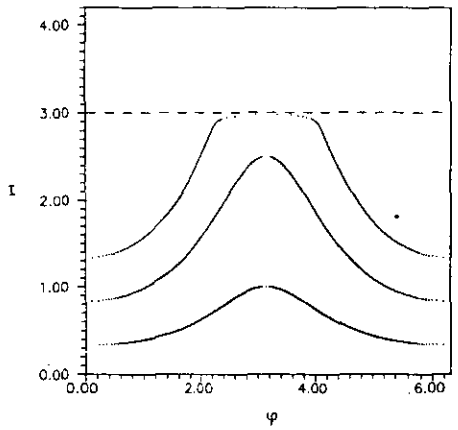

Figure 3. The same level curves of figure 1 for the smooth Hamiltonian given by (3.5). Here $A = 5.0$ and $\lambda^{-1} = 15$. Notice that, contrary to figure 2, no equilibrium points have been generated.

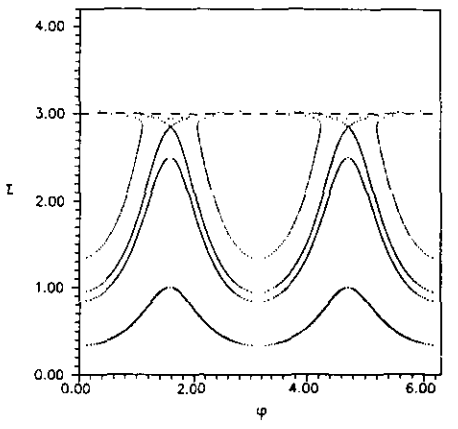

Figure 4. $I \times \varphi$ level curves for the smooth 'double hump' Hamiltonian (3.7) with $\lambda^{-1} = 15$. In this case two hyperbolic points have been created and the original (non-truncated) orbit has split in two parts.

with solutions $\varphi_f = 2\pi - \varphi_i$, $\pi - \varphi_i$, $\pi + \varphi_i$. To obtain the right solution we must find the values of φ corresponding to the tangencies of the level curves with $I = \mathcal{I}$. In this case, $dI/d\varphi = 0$ with $d^2I/d\varphi^2 < 0$ gives $\varphi_1 = \pi/2$ and $\varphi_2 = 3\pi/2$. Any orbit hitting the border must be confined between those angles, and that defines the jump: if $\varphi_1 < \varphi_i < \varphi_2$, then $\varphi_1 < \varphi_f < \varphi_2$ and if $\varphi_i < \varphi_1$, $\varphi_f > \varphi_2$.

It is clear that if we replace $\cos 2\varphi$ by $\cos n\varphi$, a chain of n islands will appear and the above results are immediately extended.

4. Two-dimensional action billiards

How does the system bounce from the billiard wall in the general case of more than one freedom? Evidently, we cannot take over the standard rule that equates the *angle of incidence with the angle of reflection from common billiards*, but the supporting principle can be generalized: this is that coordinates in the neighbourhood of a bounce point of the boundary can be found such that the collision takes place instantaneously in one canonical pair of coordinates, while the others remain fixed. In the case of a Hamiltonian of the form $p^2/2 + V(q)$ with $dV/dq \to \infty$ we obtain the reversal $p \to -p$, so $\dot{q} \to -\dot{q}$. Since the other velocities remain instaneously constant, specular reflection results.

In the general case of an action angle Hamiltonian, the boundary will be given by

$$f(\boldsymbol{I}) = 0 \tag{4.1}$$

which may be linearized around any of its points as

$$\boldsymbol{\omega} \cdot \boldsymbol{I} = \mathcal{I}. \tag{4.2}$$

Of course, the coefficients $\boldsymbol{\omega}$ and $\mathcal{I}$ are only determined within a constant, but we shall choose this so that the right-hand side of (4.2) represents I'_L, one of the L new

actions resulting from the *orthogonal transformation* $\boldsymbol{I} \rightarrow \boldsymbol{I}'$. As is well known [9], in this instance of a point transformation we obtain a full canonical transformation by simply applying an identical transformation to the corresponding angles $\boldsymbol{\varphi} \rightarrow \boldsymbol{\varphi}'$. Thus, near a given bounce point, we obtain the Hamiltonian for the billiard that generalizes (2.16) as

$$H_\lambda(\boldsymbol{I}, \boldsymbol{\varphi}) = H(\boldsymbol{I}, \boldsymbol{\varphi})[\Theta_\lambda(\mathscr{I} - \boldsymbol{\omega} \cdot \boldsymbol{I})]^2 \tag{4.3}$$

or, in the new coordinates,

$$H_\lambda(\boldsymbol{I}', \boldsymbol{\varphi}') = H(\boldsymbol{I}', \boldsymbol{\varphi}')[\Theta_\lambda(\mathscr{I} - I_L')]^2. \tag{4.4}$$

To determine the outcome of the collision with the boundary in the limit $\lambda \rightarrow 0$, we merely keep the variables $I_1', \ldots, I_{L-1}', \varphi_1', \ldots, \varphi_{L-1}'$ fixed and ascertain which branch of the phase curve the system jumps to, for the one-dimensional problem analysed in section 3.

The discussion above resolves the problem of boundary collisions for billiards of any dimension. In the important case of two-dimensional billiards we will now consider the situation where $I_2 = \mathscr{I}_2$ determines a wall, i.e.

$$H_0(\boldsymbol{I}, \boldsymbol{\varphi}; \mathscr{I}_2) = \begin{cases} H(\boldsymbol{I}, \boldsymbol{\varphi}) & (I_2 \leqslant \mathscr{I}_2) \\ 0 & (I_2 > \mathscr{I}_2). \end{cases} \tag{4.5}$$

Then, at the boundary $\dot{\varphi}_2$ receives an impulse proportional to $\delta(I_2 - \mathscr{I})$, while all the other phase velocities remain finite. By energy conservation the initial φ_{2i} and the final φ_{2f} must satisfy

$$H(I_{1i}, \mathscr{I}_2, \varphi_{1i}, \varphi_{2i}) = H(I_{1i}, \mathscr{I}_2, \varphi_{1i}, \varphi_{2f}). \tag{4.6}$$

The possibility of stable and unstable equilibria appearing in the reduced Hamiltonian $H(I_2, \varphi_2; I_{1i}, \varphi_{1i})$ now has interesting consequences. These are orbits of the original (non-truncated) Hamiltonian and, therefore, will not generally be periodic (separable Hamiltonians being an exception). These equilibria are the locus of orbit collisions where φ_2 does not jump, so they correspond to tangencies in common billiards. The hyperbolic fixed point is the limit of orbits that do not collide with the wall, analogous to orbits that glance off a dent within a concave billiard. The orbits in the neighbourhood of the elliptic point collide repeatedly with the wall and hence correspond to 'whispering gallery orbits' of convex billiards. Thus, the non-trivial dynamics within the action billiard allows for analogies to zero-angle bounces which appear only in distinct types of common billiards.

We can now truncate in the I_1 direction as well. Assuming that a generic orbit will not hit the boundaries at $\mathscr{I}_1$ and $\mathscr{I}_2$ simultaneously, the above considerations are naturally extended for the I_1 variable. Therefore, the projection of an orbit in the $I_1 \times I_2$ plane will look like a billiard, as shown schematically in figure 5(*a*).

The expected behaviour in the planes $I_1 \times \theta_1$ and $I_2 \times \theta_2$ is displayed in figures 5(*b*) and 5(*c*).

Notice that the jump at the collision points takes the initial orbit to a different orbit of the original (non-truncated) system at the same energy surface.

Here we can also define a smooth version of H_0 (by simplicity we assume that the cut-off is only in I_2):

$$H_\lambda = H(\boldsymbol{I}, \boldsymbol{\varphi})\Theta_\lambda^2(\mathscr{I} - I_2). \tag{4.7}$$

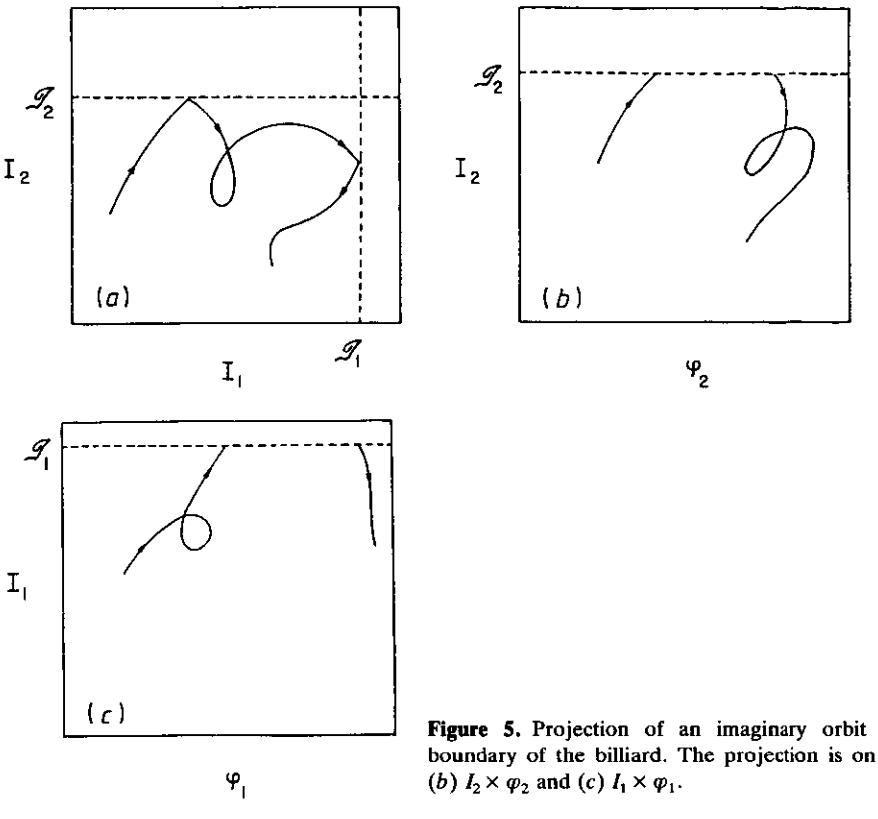

Figure 5. Projection of an imaginary orbit hitting the boundary of the billiard. The projection is on (*a*) $I_1 \times I_2$, (*b*) $I_2 \times \varphi_2$ and (*c*) $I_1 \times \varphi_1$.

In this case, the 'whispering orbits' turn into smooth curves that wander very close to $I_2 = \mathcal{I}$ but with φ_2 changing very fast. Depending on the coupling of φ_2, this can cause the other variables to oscillate rapidly (see the example below). Besides this 'soft whispering gallery', there will also be orbits that, coming fom other regions of phase space, approach the elliptic point and leave after having spent an arbitrary amount of time trapped among the whispering orbits. By continuity, these orbits must also exist in the limit $\lambda \to 0$. This fact suggests the possible existence of structures analogous to Cantori around the elliptic point.

As an application of the ideas and methods developed above we chose the Hamiltonian originated in the normal form expansion around a 3:1 resonance [6, 9]. Truncating this expansion so as to get an integrable approximation near the resonance yields

$$H(J, \theta) = (\tfrac{1}{3} - \lambda)J_1 + J_2 + \sum_{n+m=2}^{2} C_{nm} J_1^n J_2^m + \alpha J_1^{3/2} J_2^{1/2} \cos(3\theta_1 - \theta_2) \quad (4.8)$$

where λ measures how far off-resonance the system is. Choosing $C_{11} = C_{02} = 0$, $C_{20} \equiv \gamma$ and adding an extra term to break integrability gives

$$H(J, \theta) = (\tfrac{1}{3} - \lambda)J_1 + J_2 + \gamma J_1^2 + \alpha J_1^{3/2} J_1^{1/2} \cos(3\theta_1 - \theta_2) + \beta J_1 J_2 \cos 2\theta_2. \quad (4.9)$$

The quantization of this Hamiltonian is then obtained by using (2.4) and (2.6).

Therefore, to the variables $(\boldsymbol{J}, \boldsymbol{\theta})$ there corresponds a set of basis states $|n_1 n_2\rangle$ in the sense of (2.7).

To these action and angle variableless we associate regular $(\boldsymbol{p}, \boldsymbol{q})$ Cartesian coordinates by inverting the transformations (2.2) and (2.4):

$$p_i = \sqrt{2J_i}\cos\theta_1$$
$$q_i = \sqrt{2J_i}\sin\theta_i \qquad i = 1, 2.$$

The Poincaré sections for this system will be presented in the above variables (instead of $(\boldsymbol{J}, \boldsymbol{\theta})$ or $(\boldsymbol{I}, \boldsymbol{\varphi})$—see below) for the sake of clarity. However, it is convenient for classical puposes to make the canonical transformation $(\boldsymbol{J}, \boldsymbol{\theta}) \rightarrow (\boldsymbol{I}, \boldsymbol{\varphi})$, generated by

$$S(\boldsymbol{\theta}, \boldsymbol{I}) = I_1(3\theta_1 - \theta_2) + I_2(2\theta_2). \tag{4.10}$$

This takes (4.9) into

$$H(\boldsymbol{I}, \boldsymbol{\varphi}) = H_0 + \alpha H_1 + \beta H_2 \tag{4.11}$$

where

$$H_0 = 3\lambda I_1 + 2I_2 + 9\gamma I^2$$
$$H_1 = 3\sqrt{3} I_1^{3/2}\sqrt{2I_2 - I_1}\cos\varphi_1$$
$$H_2 = 3I_1(2I_2 - I_1)\cos\varphi_2.$$

If $\beta = 0$, the system is integrable and I_2 is conserved. Figure 6 shows a Poincaré section at $\varphi_2 = 0$ and the 3:1 unstable periodic orbit, together with its stable and unstable manifolds. The quantum mechanical version of this problem has the Hamiltonian matrix decoupled into finite blocks of constant I_2. When β is switched on, these blocks are coupled but remain finite. In this case it is enough to truncate the matrix by limiting I_2 to a maximum value. Classically, the same is true due to the square root factor $\sqrt{2I_2 - I_1}$: if I_2 is limited to $\mathcal{I}$, $I_1 \leqslant 2\mathcal{I}$, and the billiard will have a triangular shape, as shown in figure 7.

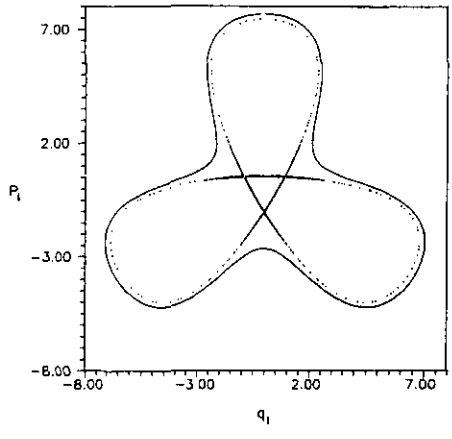

Figure 6. Poincaré section of the separatrices at $q_2 = 0$ for $\beta = 0$ and $E = 11.0$. The full curve is the projection of the surface $I_2 = 5.80$ at the same energy.

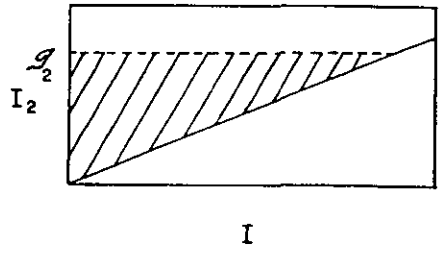

Figure 7. Billiard shape for the Hamiltonian of (4.11).

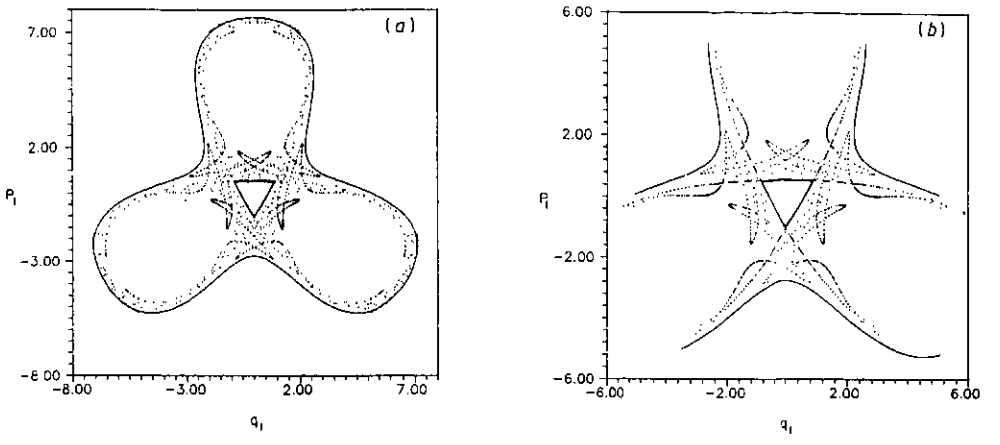

Figure 8. (*a*) Poincaré section of the separatrices as in figure 6 but for $\beta = 0.003$. Notice that the separatrices hit the continuous line only far from the periodic orbit. (*b*) Enlargement of (*a*) showing the winding of the separatrices.

Figure 6 also shows the curve corresponding to $I_2 = \mathcal{I} = 5.8$. Therefore, for $\beta = 0$, the orbits of H_0 are exactly the same as for H, except that all orbits having $I_2 > \mathcal{I}$ are omitted, but no trajectory ever *hits* the boundary, since I_2 is a constant of motion.

For $\beta \neq 0$, the separatrices do not join smoothly and start to zig zag near the hyperbolic points. This is shown in figure 8, where the boundary at $\mathcal{I}_2 = 5.8$ also appears. We see that, in this case, the separatrices hardly cross the 'billiard wall' and no big changes are expected for H_0. In figure 9 $J = 5.6$ and, therefore, we can forecast some changes in the analogous curve of H_0.

Before showing the separatrices of H_0 for different values of $\mathcal{I}$, we define the smooth Hamiltonian H_λ as in (4.7). Figure 10 displays a comparison between the orbits of H, H_0 and H_λ for three different values of λ. It is important to notice that we had to use a time step four times smaller in order to achieve the same numerical precision in the orbits of H_λ that we obtained for the orbits of H or H_0, This is due to the strong nonlinearity near $I_2 = \mathcal{I}$. If the orbits shown in figure 10 were to be integrated for larger times, the time step would have to be progressively diminished.

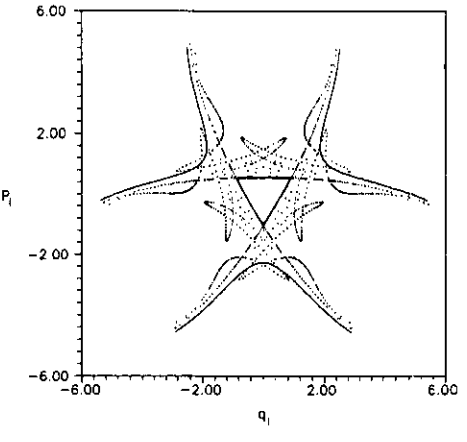

Figure 9. Enlargement as in figure 8(*b*) but with the full line showing the surface at $I_2 = 5.60$. Notice that now this 'boundary' intersects the separatrices much earlier than before.

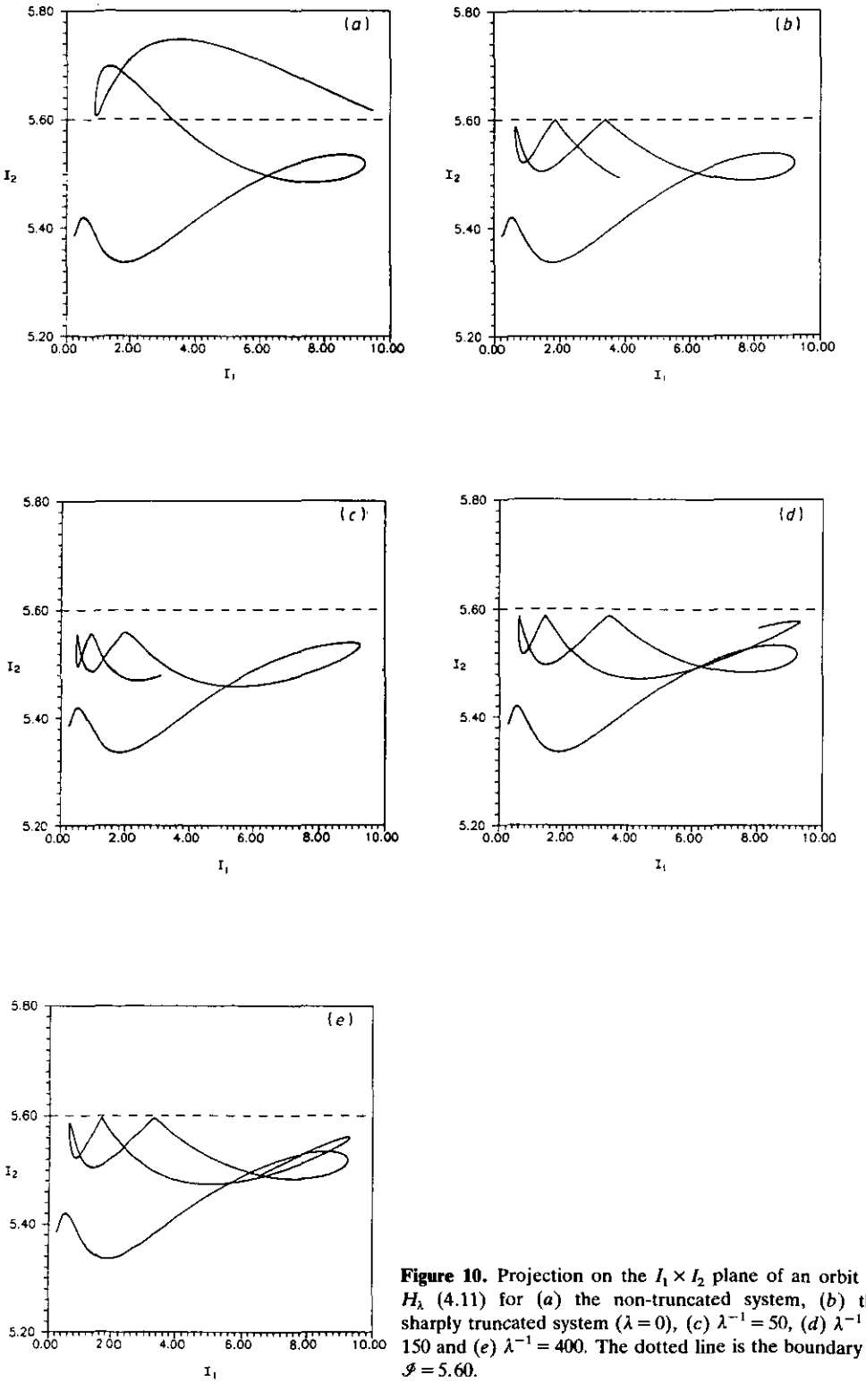

Figure 10. Projection on the $I_1 \times I_2$ plane of an orbit of H_λ (4.11) for (*a*) the non-truncated system, (*b*) the sharply truncated system ($\lambda = 0$), (*c*) $\lambda^{-1} = 50$, (*d*) $\lambda^{-1} = 150$ and (*e*) $\lambda^{-1} = 400$. The dotted line is the boundary at $\mathscr{I} = 5.60$.

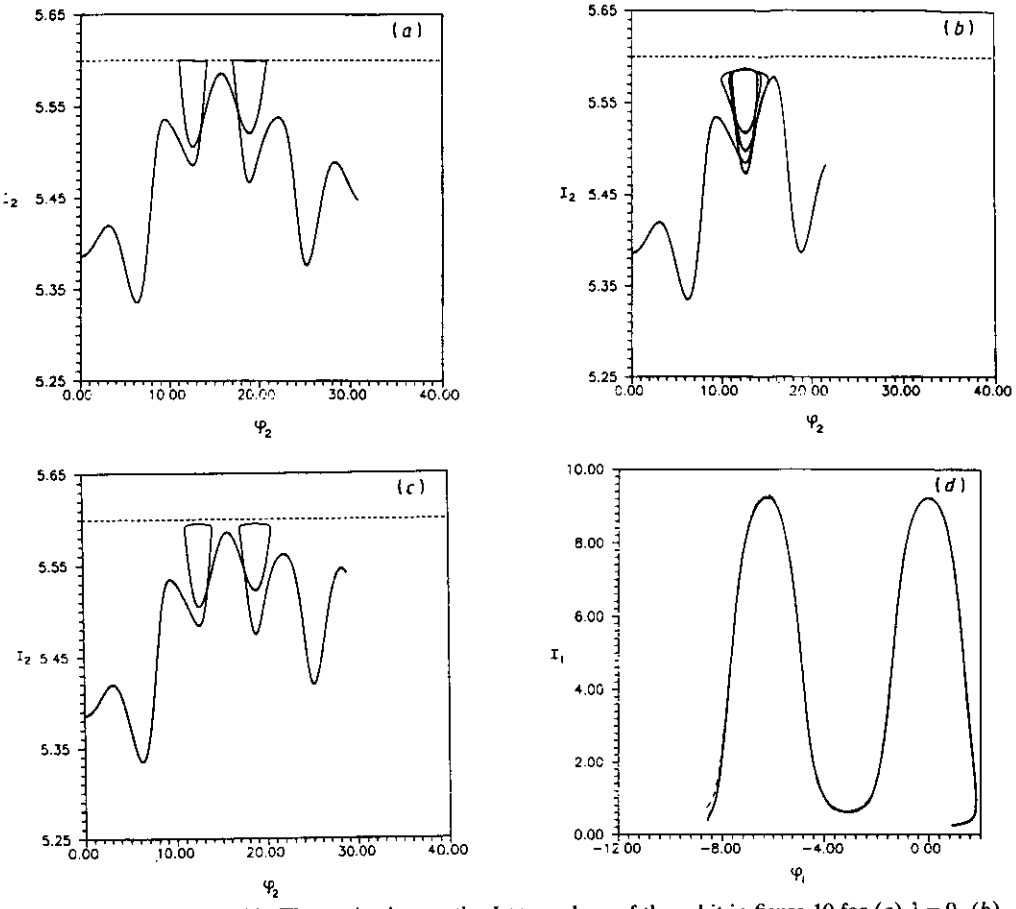

Figure 11. The projection on the $I_2 \times \varphi_2$ plane of the orbit in figure 10 for (*a*) $\lambda = 0$, (*b*) $\lambda^{-1} = 150$ and (*c*) $\lambda^{-1} = 400$. (*d*) The $I_1 \times \varphi_1$ projection for the three situations above. The full curve represents $\lambda = 0$, the short-broken curve $\lambda^{-1} = 150$ and the long-broken $\lambda^{-1} = 400$.

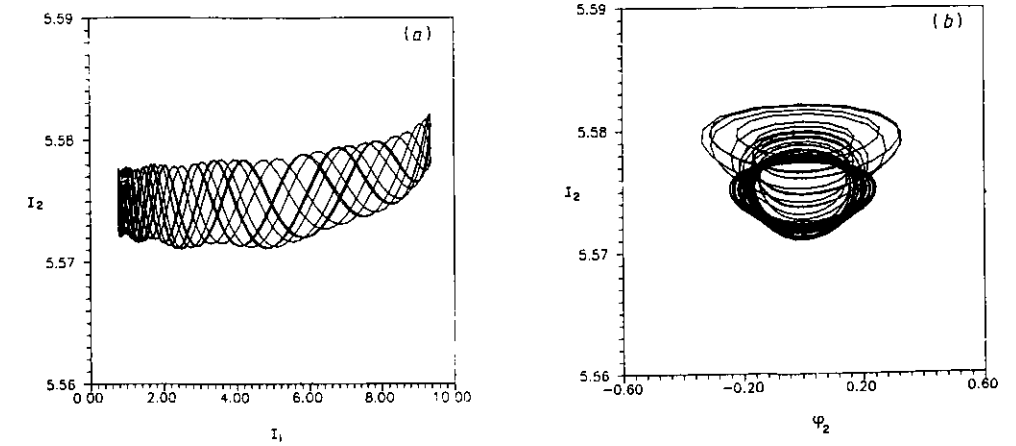

Figure 12. Soft whispering orbit projected on (*a*) $I_2 \times I_1$ and (*b*) $I_2 \times \varphi_2$ planes for $\lambda^{-1} = 150$.

This makes it very hard to calculate precise Poincaré sections of H_λ. In Figure 11 we show the projection of the same orbit in the $J_2 \times \varphi_2$ plane (parts a–c) and in the $J_1 \times \varphi_1$ plane (part d). This figure indicates that for a large enough value of λ this orbit gets trapped in the 'island' generated by the smooth step function, as discussed before. As λ is decreased, the trapping disappears and the motion tends to that of H_0. Another interesting feature is the smoothness of the $I_1 \times \varphi_1$ projections. The three curves of (a–c) of figure 11 almost coincide in this projection.

An example of a 'soft whispering' orbit is shown in figure 12 for a fairly smooth Hamiltonian ($\lambda^{-1} = 150$). The orbit appears to be on a torus, but this is probably not so, as can be seen by the accumulation of windings near the left side of the plot. Figure 13 shows projection on the $I_1 \times I_2$ plane of the same orbit (same initial conditions) for a smaller λ. There, it is clear that a torus does not support the orbit since a very complex structure appears. In figure 13(c) the whispering orbit is shown for $\lambda = 0$ (sharply truncated system).

Finally, in figure 14 we show the Poincaré section of the separatrices of H_0 for various values of $\mathcal{I}$. To understand these figures, consider a small segment of the separatrix near one of the hyperbolic points and evolve it in time as sketched in figure 15. Suppose that this segment does not reach $I_2 = \mathcal{I}$ during its first loop back to the section and that the points on the nearby segment all touch $I_2 = \mathcal{I}$ at some

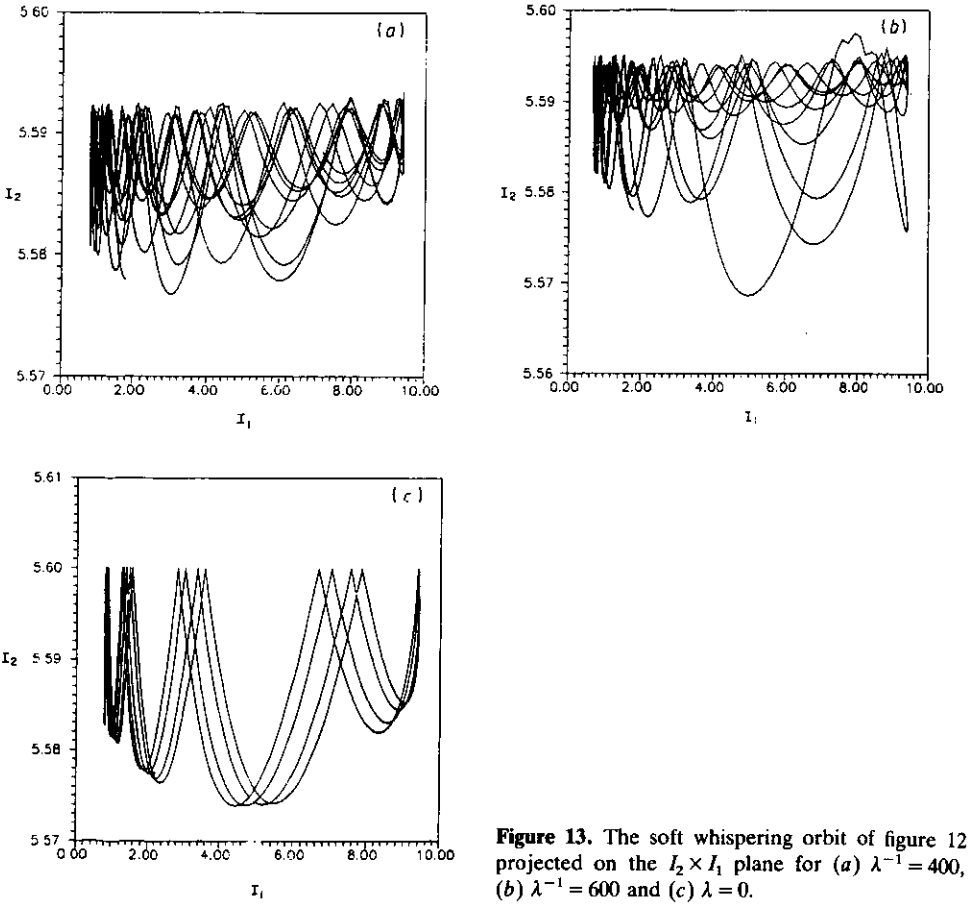

Figure 13. The soft whispering orbit of figure 12 projected on the $I_2 \times I_1$ plane for (a) $\lambda^{-1} = 400$, (b) $\lambda^{-1} = 600$ and (c) $\lambda = 0$.

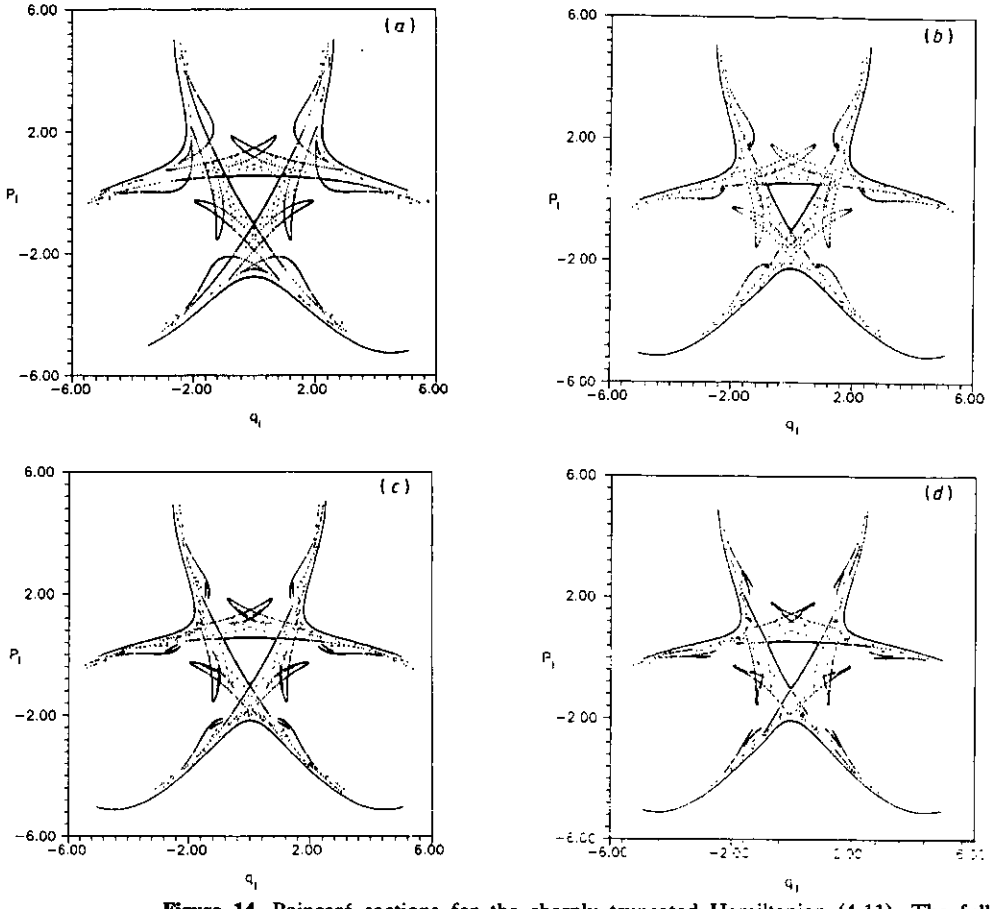

Figure 14. Poincaré sections for the sharply truncated Hamiltonian (4.11). The full curve represents the boundary at $I_2 = \mathcal{I}$ for (*a*) $\mathcal{I} = 5.8$, (*b*) $\mathcal{I} = 5.6$, (*c*) $\mathcal{I} = 5.575$ and (*d*) $\mathcal{I} = 5.55$.

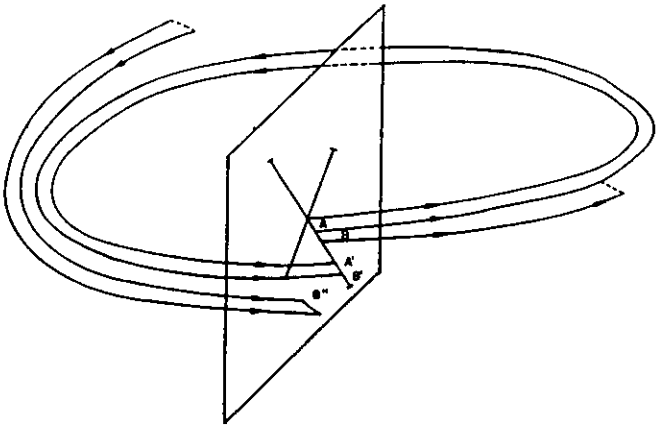

Figure 15. Schematic Poincaré section showing the orbits hitting the boundary. The orbits on segment *A* do not hit the boundary and are mapped onto *A'*. The orbits on the segment *B* hit the boundary (each at a different point), jumping to other orbits that finally hit the section at B″.

point. Then, instead of falling at the separatrices of H, each point will jump to a different curve on its way around. Therefore, we expect to see holes in what were the sepatrices of H plus a set of disconnected curves. This is exactly what is shown in figure 12. As λ decreases, more and more holes and pieces of curves appear.

5. Conclusions

It is not yet clear whether there is any intrinsic value in the study of action billiards for classical mechanics. For quantum mechanics, it may be argued that the concept in itself is more important than the details of the consequent classical motion, since for a large range of energies the orbits may be wholly unaffected by the billiard walls. This is the classical basis for the computational evidence that a certain proportion of eigenvalues and eigenvectors often remain invariant with respect to truncations of the Hamiltonian matrix. One of the main points of this paper is that it is now unnecessary to seek convergence of the truncation process.

In many cases where truncation in quantum mechanics provides a good approximation, action billiards merely supply a better justification for existing practice. However, it is now valid to truncate even systems where this procedure is wholly unstable. This will be the case when most orbits hit the walls, as with common billiards. In such cases it will then be fundamental to understand the classical motion in the manner that we have presented here.

Finally, we point out that the present analysis has supplied us with a fascinating example where different classical systems, with diverse orbit topologies, correspond to the same Hamiltonian matrices in quantum mechanics. Of course, it must be noted that this duplicity depends on fixing a finite value for Planck's constant. Thus the different manners of smoothly cutting off the Hamiltonian outside the billiard are not identical. If the boundary volume is narrow with respect to $\hbar^L$, the Hamiltonian matrices for both cases coincide. Nonetheless, in the semiclassical limit, for a fixed classical cut-off function, the Hamiltonian matrices for both cases will exhibit the classical differences as $\hbar \to 0$.

Acknowledgments

We thank Dr C P Malta and Dr R E Carvalho for helpful discussions. Financial support from FAPESP, CNPq and FINEP is gratefully acknowledged.

References

[1] Hannay J H and Berry M V 1980 *Physica* **1D** 267
[2] Balazs N and Voros A 1989 *Ann. Phys., New York* **190** 1
[3] Leboeuf P and Saraceno M 1990 *J. Phys. A: Math. Gen.* **23** 1745
[4] Percival I C and Richards D 1970 *J. Phys. B: At. Mol. Phys.* **3** 1035
[5] Ozorio de Almeida A M 1984 *Rev. Bras. Fis.* **14** 62
[6] Arnold V I 1978 *Mathematical Methods of Classical Mechanics* (New York: Springer)
[7] Springborg, M 1983 *J. Phys. A: Math. Gen.* **16** 536
[8] Messiah A 1980 *Quantum Mechanics* (Amsterdam: North-Holland)
[9] Ozorio de Almeida A M 1988 *Hamiltonian Systems: Chaos and Quantization* (Cambridge: Cambridge University Press)